

CrossMark
click for updates

Cite this: DOI: 10.1039/c6cy00858e

Crotonaldehyde hydrogenation on platinum–titanium oxide and platinum–cerium oxide catalysts: selective C=O bond hydrogen requires platinum sites beyond the oxide–metal interface†

Xin Yang, Yutichai Mueangern, Quinn A. Baker and L. Robert Baker*

We have investigated a series of Pt–TiO₂ and Pt–CeO₂ catalysts for crotonaldehyde hydrogenation with the goal of better understanding the kinetics of C=O bond hydrogenation. It has been established that in these systems, Pt is the active phase for C=C bond hydrogenation, while the interface between Pt and an active metal oxide is required for selective C=O bond hydrogenation. In this work we demonstrate that in addition to the presence of an active oxide–metal interface, there is also a need for accessible Pt sites beyond this interface to facilitate C=O bond hydrogenation. Passivating Pt with TiO₂ at coverages approaching unity is shown to decrease the rate of C=O bond hydrogenation in exact proportion to the rate of C=C bond hydrogenation, suggesting that both pathways become rate limited by the accessible Pt surface area at high oxide coverage. A similar kinetic result is demonstrated for CeO₂ nanocubes deposited on a Pt film, where the rate of C=O bond hydrogenation initially increases with CeO₂ nanocube coverage and then decreases again at high CeO₂ coverage, even though the nanocubes remain discrete. Because the density of interface sites scales linearly with the coverage of CeO₂ nanocubes on the Pt surface, this decrease in activity shows that accessible Pt sites rather than oxide–metal interface sites become rate limiting for C=O bond hydrogenation at high oxide coverage. Finally, in bilayer catalysts of CeO₂ and Pt nanocubes, we find that both Pt-on-CeO₂ and CeO₂-on-Pt are active for C=C bond hydrogenation, while only Pt-on-CeO₂ is active for C=O bond hydrogenation. These results are discussed in terms of a spillover-mediated reaction mechanism in which a reaction intermediate must diffuse either to or across the active oxide–metal interface in order to promote C=O bond hydrogenation.

Received 20th April 2016,
Accepted 28th April 2016

DOI: 10.1039/c6cy00858e

www.rsc.org/catalysis

1. Introduction

Understanding the mechanism of catalytic selectivity on surfaces is critical for efficient chemical processing of limited natural resources. In previous decades, catalysis research has focused largely on optimizing catalytic activity. However, the reality of limited natural resources, the economic uncertainty of petroleum-derived feedstocks, and a better understanding of the environmental impact of unwanted chemical byproducts all argue for a shift in research focus from catalytic activity toward catalytic selectivity.^{1–3} However, the selectivity of heterogeneous nanoparticle catalysts is often challenging to control since catalyst performance relies on carefully optimizing the surface properties of complex systems,^{4,5} often involving both metallic and oxide phases.^{6,7} Additionally, design

parameters for catalyst optimization are frequently lacking because of the difficulty associated with studying reaction mechanisms on such complex bifunctional surfaces.

The role of an oxide support represents an important factor that governs catalytic performance for many heterogeneous reactions including low temperature CO oxidation on Au,^{8–10} selective oxidation of alkenes to epoxides,¹¹ selective oxidation of molecular oxygen to peroxide,^{12,13} hydroformylation of olefins to aldehydes,¹⁴ and selective partial hydrogenation of aldehydes and ketones.^{15–19} In recent studies by Kennedy *et al.*, the kinetics of Pt nanoparticles supported on inactive SiO₂ and on active TiO₂ were compared.²⁰ It was found that dispersing Pt nanoparticles on SiO₂ led to activity consistent with reported kinetics for single crystal Pt.²¹ However, dispersing the same Pt nanoparticles on TiO₂ led to a dramatic increase in the rate of C=O bond hydrogenation compared to SiO₂-supported particles.

The mechanism of selective C=O bond hydrogenation was also investigated using sum frequency generation (SFG) vibrational spectroscopy to probe the reaction intermediates

The Ohio State University, Department of Chemistry and Biochemistry, Columbus, OH 43210, USA. E-mail: baker.2364@osu.edu; Tel: +(614) 292 2088

† Electronic supplementary information (ESI) available. See DOI: 10.1039/c6cy00858e

present on various surfaces during reaction conditions.^{20,22} The results of these studies indicate that selective C=O bond activation occurs specifically on the oxide surface *via* an electron transfer interaction leading to the observation of an alkoxy intermediates bonded to the oxide *via* the carbonyl O. This alkoxy species was observed both for crotonaldehyde²⁰ and furfuraldehyde²² on a TiO₂ surface. However, it was also determined that this species did not lead to active turnover of an alcohol product (*i.e.* crotyl alcohol or furfuryl alcohol, respectively) except when a Pt nanoparticle catalyst was also present on the oxide surface and the Pt nanoparticles were in direct contact with the TiO₂ surface, which only occurred following removal of an organic capping agent. From these observations it was concluded that C=O bond activation occurs on the oxide phase of a bi-functional catalyst while H dissociation occurs on the Pt phase, and that catalytic activity requires the spillover of one or more of these active species either to or across the oxide–metal interface.

This study also found that in addition to enhancing the rate of C=O bond hydrogenation, the rate of C=C bond hydrogenation is also slightly increased in the Pt–TiO₂ catalyst relative to the Pt–SiO₂ system, although the effect of the support on C=C bond hydrogenation kinetics was less dramatic than for C=O bond hydrogenation kinetics. This observation was explained by the ability of pure Pt to directly catalyze C=C bond hydrogenation as well as its ability to promote the isomerization of crotyl alcohol to the thermodynamically favored butyraldehyde product as shown in Scheme 1. Consequently, although the Pt-on-TiO₂ catalyst is much more active for C=O bond hydrogenation than Pt-on-SiO₂, it cannot yield high selectivity for partial C=O bond hydrogenation because of the inability to turn off the competing C=C bond hydrogenation pathway that is catalyzed by Pt alone.

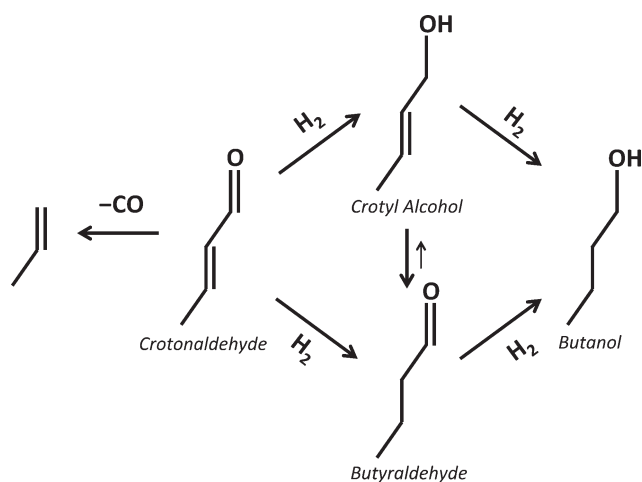
Toward the goal of demonstrating high selectivity for C=O bond hydrogenation in the absence of competing C=C bond chemistry, we have investigated the inverse catalyst structure, *i.e.* metal–oxide–on–metal as opposed to metal–on–metal–oxide.^{23–25} The motivation for this design has to do

with the proposed active site for selective C=O bond hydrogenation. Because Pt alone catalyzes C=C bond hydrogenation, while both Pt and an active metal oxide are required to catalyze C=O bond hydrogenation, it has been hypothesized that C=C bond hydrogenation occurs on the Pt surface, while C=O bond hydrogenation occurs at the 3-phase boundary defined by the oxide–metal interface or possibly on the oxide surface directly following the spillover of atomic H from the Pt phase. This assignment of active sites suggests that a selectivity difference may be observed for the oxide–on–metal catalyst compared to inverse metal–on–oxide case. This is because as an oxide phase passivates a Pt surface, the rate of C=C bond hydrogenation would decrease in proportion to the decreasing area of exposed Pt. On the other hand the rate of C=O bond hydrogenation would instead scale with the number of sites along the oxide–metal interface. At oxide coverages approaching unity, both types of active sites approach zero; however, the ratio of interface to bulk Pt sites should increase dramatically as essentially every exposed Pt atom becomes located at or near a TiO₂ interface.

This idea has already been explored in part by Boffa *et al.*, who studied the kinetics for CO and CO₂ hydrogenation on a planar Rh catalyst as a function of coverage by various metal oxides.^{23–25} In these studies it was shown that a maximum rate enhancement occurs at 50% oxide coverage on the Rh catalyst, and from this, it was concluded that the oxide–metal interface was the active site for CO and CO₂ hydrogenation on the oxide-decorated Rh catalyst because the number of interface sites are maximized at a coverage equal to 50% of a monolayer. However, this work only measured the rates of single path reactions. In the case of a multipath reaction, such as crotonaldehyde hydrogenation, it is conceivable that above 50% oxide coverage the total number of exposed metal sites may decrease more rapidly than the number of oxide–metal interface sites, suggesting that catalytic selectivity may be increased at the expense of overall activity at high oxide coverage. Consequently, this work builds on earlier findings by Boffa *et al.* by extending this work to a study of partial hydrogenation selectivity in a multipath reaction.

Additionally, we note that it was not possible in previous studies to independently vary the number of interface sites and the total number of exposed metal sites, which both decreased with increasing oxide coverage above 50% of an oxide monolayer. In this work, we begin by investigating TiO₂ films grown on Pt by atomic layer deposition (ALD), which is similar to the previous studies in that the density of interface sites to total Pt sites is qualitatively predicted as a function of coverage, but it is not actually controlled. Importantly however, we additionally report the effect of oxide coverage by discrete CeO₂ nanocubes deposited by Langmuir–Blodgett deposition on a Pt surface. Because the CeO₂ nanocubes remain discrete, even at high coverage, this latter approach allows us to increase the number of interface sites on a Pt surface while decreasing the total number of exposed metal sites.

Although we had hoped that this approach would lead to a highly selective catalyst for partial hydrogenation of



Scheme 1

crotonaldehyde to crotyl alcohol by maximizing the ratio of interface sites to the total number of Pt sites, we show here that this is not the case. In fact we demonstrate using 3 different catalyst systems consisting of both TiO₂ on Pt and CeO₂ on Pt, that the rate of C=O bond hydrogenation becomes limited by Pt surface area at high oxide coverage. From this we do not conclude that Pt is necessarily the actual site of selective C=O bond hydrogenation. Instead we conclude that at least one step in the reaction sequence leading to selective C=O bond hydrogenation occurs the Pt surface area near the active interface and that the kinetics of this step becomes rate limiting at high oxide coverage. Specifically, this step may represent the dissociation of molecular H₂, which is known to occur much more efficiently on Pt compared to a metal oxide. According to this mechanism, H₂ dissociation on Pt is followed by the surface diffusion of atomic H to the oxide–metal interface where it subsequently reacts with activated crotonaldehyde to produce crotyl alcohol. This mechanism suggests that Pt sites near the metal oxide are required to provide a sufficient supply of atomic H to the active oxide–metal interface for selective C=O bond hydrogenation to occur.

It is also known that H spillover from the Pt catalyst to the metal oxide is responsible for surface reduction of the oxide,^{26,27} which is critical to activate the catalyst for selective C=O bond hydrogenation. The importance of H to activate the metal oxide phase is consistent with recent experimental and theoretical observations that the charge–transfer interaction between crotonaldehyde and the catalyst leading to selective C=O bond activation occurs at an O vacancy site on the oxide surface.²² Consequently, for catalysts with only a small amount of exposed Pt, it is likely that there is insufficient H spillover to adequately activate the oxide surface by the formation of O vacancies.

As an alternate hypothesis, we consider the possibility that the formation of crotyl alcohol may actually occur on Pt following the reverse spillover of a crotyl-oxy intermediate, previously identified on a TiO₂ surface by SFG vibrational spectroscopy.²⁰ This crotyl-oxy intermediate that forms on TiO₂ has been hypothesized to be the surface precursor for crotyl alcohol during crotonaldehyde hydrogenation on a Pt–TiO₂ catalyst. Consequently, it is possible that this species, which forms on a TiO₂ surface, may migrate across the oxide–metal interface onto the Pt catalyst where it subsequently reacts to form crotyl alcohol. Here the distance that the crotyl oxy intermediate migrates from the oxide–metal interface is determined by its diffusional mean-free path on Pt under reaction conditions. Fig. S1 in the ESI† shows an approximate calculation of the root-mean-square distance for surface diffusion given a range of activation barriers for surface hopping. Taking one divided by the turnover frequency as an estimate of the reactant's lifetime on the catalyst surface, we see that if reasonable values of hopping frequency, hopping barrier, and relative surface coverage are assumed, that at a reaction temperature of 100 °C it is possible for an intermediate to easily diffuse >10 nm on the catalyst surface during re-

action. The purpose of this calculation is not to estimate an actual diffusion length for a specific reaction intermediate, but rather to demonstrate the feasibility of diffusion on this length scale during catalytic reaction. Although this mechanism admittedly breaks with the predominant belief that the oxide–metal interface is the active site for selective C=O bond hydrogenation, this reaction pathway could explain the both dependence of catalytic selectivity on oxide electronic structure^{23,25} since the metal oxide is responsible for formation of the active crotyl-oxy intermediate as well as the need for an active oxide–metal interface since this interface is required for the reverse spillover of crotyl-oxy from TiO₂ (or CeO₂) to Pt.

2. Experimental

2.1. Catalyst preparation

Atomic layer deposition of TiO₂ overlayers on Pt nanoparticle catalysts. Pt nanocubes were synthesized following a previously reported protocol.²⁸ To summarize, 0.025 mmol of H₂Pt(IV)Cl₆·6H₂O, 0.025 mmol of (NH₄)₂Pt(II)Cl₄, 0.75 mmol of tetramethylammonium bromide (TMAB), and 1.0 mmol of polyvinylpyrrolidone (PVP) with a repeating mass unit of 29 000 g mol⁻¹ were dissolved in 10 mL of ethylene glycol inside a 25 mL round bottom flask. A balloon was used to keep the round bottom flask under a blanket of argon. The reaction mixture was heated to 180 °C and held at this temperature for 20 min. During this time the solution color changed from clear to black. After 20 min, the reaction mixture was allowed to cool to room temperature, and the crude solution was transferred to a centrifuge tube and mixed with 90 mL of acetone. The solution was then centrifuged at 3000 rpm for 10 minutes, and the black precipitate was collected. Three ethanol/hexane wash steps were performed to remove excess capping agent. Each wash consisted of dispersing the Pt nanoparticles in 20 mL of ethanol followed by precipitation with 80 mL of hexanes and centrifugation at 8700 rpm. Following the final wash step, the nanoparticle pellet was dispersed in 10 mL of ethanol. Fig. 1A shows a TEM image of the synthesized Pt nanocubes drop cast onto a lacey carbon film.

For kinetic studies of crotonaldehyde hydrogenation, the synthesized Pt nanoparticles were deposited by Langmuir–Blodgett (LB) deposition onto a Si (100) wafer with a 500 nm thermal oxide layer. Prior to deposition the SiO₂ substrate was treated with No-Chromix, a commercial agent used to remove organic contaminants and to render the surface hydrophilic. This cleaning solution was prepared by dissolving 10 grams of No-Chromix in 15 mL of concentrated sulfuric acid. For cleaning, the SiO₂ sample was placed in the No-Chromix solution and heated to 80 °C for 1 hour. Following nanoparticle deposition by LB, samples were exposed to UV irradiation for 3 hours to remove the PVP capping agent following a previously established protocol.²² The UV light source employed consists of two low-pressure Hg lamps (Light Sources Inc., model GPH357T5VH/4P) positioned 2.5 cm apart from each

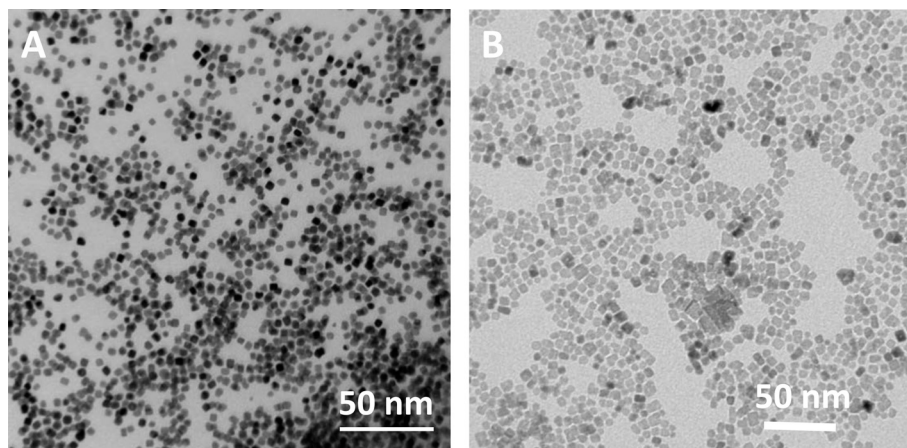


Fig. 1 TEM image of Pt nanoparticles deposited (A) and CeO₂ nanoparticles (B). For these images, Pt nanoparticles were drop cast onto a lacey carbon TEM grid while CeO₂ nanoparticles were deposited onto a lacey carbon TEM grid by LB deposition.

other in a parallel orientation. The sample was positioned at a fixed height of 1.2 cm beneath the two lamps. Following removal of the capping agent by UV ozone cleaning, a TiO₂ film was deposited onto the nanoparticle catalysts by atomic layer deposition (ALD). ALD was performed using a Picosun SUNALE R-150B system. TiO₂ films were grown using TiCl₄ and H₂O precursors. The substrate temperature was kept at 100 °C, and the exposure pulses for TiCl₄ and H₂O were 0.4 second each.

CeO₂ nanocubes on Pt thin film catalysts. In separate experiments CeO₂ nanocubes were deposited onto Pt thin film catalysts in order to investigate the kinetics of crotonaldehyde hydrogenation as function of CeO₂ nanoparticle coverage. The colloidal synthesis of the CeO₂ nanoparticles follows a previously reported method.²⁹ To summarize, 15 mL of 16.7 mM cerium(III) nitrate in water was transferred into a 50 mL Teflon-cup inside a stainless-steel autoclave reactor followed by addition of 1.5 mL of oleic acid and 0.15 mL of *tert*-butylamine. Finally, 15 mL of toluene was added to the Teflon-lined reactor, which was then sealed and placed inside a temperature-controlled oven at 180 °C for 24 hours. The resulting mixture was allowed to cool to room temperature and then centrifuged at 3000 rpm for 5 min. The upper organic layer was collected and precipitated with twice the volume of ethanol. The supernatant was discarded, and the precipitate was dispersed in 7 mL of chloroform for subsequent LB deposition.^{1,3} Fig. 1B shows a TEM image of the synthesized CeO₂ nanocubes.

A Si (100) wafer with a 500 nm thermal oxide layer served as the catalyst support. A 20 nm Pt film was deposited onto this substrate *via* electron beam evaporation. Following preparation of the Pt films, Langmuir–Blodgett deposition was used to deposit the CeO₂ nanocubes at well controlled coverages onto the Pt film.^{4,5} During LB deposition a suspension of CeO₂ oxide nanocubes in chloroform was dropped onto a water surface. The chloroform solvent was allowed to evaporate for 30 minutes leaving only the CeO₂ nanoparticles. The particle density at the water surface was controlled using two

Teflon barriers located at the ends of the trough. Surface pressure was monitored as a function of film compression during nanoparticle deposition. These experiments used a NIMA 612D Langmuir–Blodgett trough. All Pt films were treated with UV irradiation for 30 minutes prior to LB deposition to render the surface hydrophilic. Following LB deposition, the catalysts were exposed to UV irradiation for 12 hours to remove the oleic acid capping agent.

2.2. Kinetic studies of crotonaldehyde hydrogenation

Reaction kinetics were measured in a stainless steel batch mode reactor connected to an Agilent 7890B gas chromatograph (GC) equipped with a flame ionization detector. A fused silica Supelcowax capillary column was used for product separation (Supelcowax 10, 30 m × 0.32 mm × 0.5 μm). Injection sequences monitored the rate of product formation over the course of 3 hours. During reaction the catalyst temperature was fixed at 100 °C using a boron nitride substrate heater. The reaction mixture consisted of 1 Torr crotonaldehyde, 100 Torr H₂, and 659 Torr He. A metal bellows recirculation pump mixed the gas inside the chamber to ensure that the measured kinetics were not diffusion limited. Reaction rates were determined from fits to peak areas *versus* time and normalized to sensitivity factors for each product. Selectivity values were calculated as the rate of formation for each product normalized to the combined rates of all detected products.^{8,9} Error bars represent 95% confidence intervals based on linear fits to the rate of product formation *versus* time.

2.3. TEM imaging and XPS surface analysis

The coverage of CeO₂ nanocubes was characterized by transmission electron microscopy (TEM) and by X-ray photoelectron spectroscopy (XPS). Samples for TEM analysis were prepared by LB deposition onto lacey carbon film TEM grids. Prior to LB deposition, the lacey carbon films were treated under UV irradiation for 20 minutes to render the surface

hydrophilic. These grids were then placed directly next to the Pt thin film catalysts used in kinetic studies described above so that the TEM images reported here correspond directly to the nanoparticle films tested for crotonaldehyde hydrogenation. However, lacey carbon TEM grids are not compatible with the extended UV irradiation used to remove the oleic acid capping agent from the CeO₂ catalyst samples prior to kinetic measurements. Consequently, to investigate the stability of the CeO₂ nanoparticles under reaction conditions following oleic acid cap removal by UV ozone cleaning, Si₃N₄ TEM membranes were used instead. These studies showed that the CeO₂ nanoparticles did not melt or undergo significant agglomeration during reaction conditions at 100 °C. TEM imaging of the CeO₂ nanocubes was performed using a Philips CM-200 TEM microscope. The Pt nanocubes were imaged using an FEI Helios Nanolab 600 Dual Beam focused ion beam/scanning electron microscope.

XPS was also used to characterize the surface composition of the prepared catalysts. These experiments utilized a Kratos Axis Ultra XPS spectrometer with a monochromatic Al K α source (BE = 1486.6 eV) operating at 120 W with a 12 kV accelerating voltage. The base pressure generated in the ion-pumped chamber was at 1.6×10^{-9} mbar. Atomic fractions reflect the results of peak area fittings of the Pt 4f, Ti 2p, and Ce 3d peaks followed by normalization to elemental sensitivity factors.

3. Results and discussion

3.1. TiO₂ on Pt – atomic layer deposition

Scheme 1 depicts the various possible reaction pathways for crotonaldehyde hydrogenation on Pt. Three primary reaction

pathways are visible in this scheme: 1) hydrogenation of the C=C bond to form butyraldehyde, 2) hydrogenation of the C=O bond to form crotyl alcohol, and 3) decarbonylation to produce propylene. In addition, both butyraldehyde and crotyl alcohol can undergo a second hydrogenation step to form the completely saturated butanol product. Finally, crotyl alcohol can also isomerize to the thermodynamically favored butyraldehyde product. In this work we focus primarily on the selectivity between C=C and C=O bond hydrogenation.

As can be seen from Fig. 2 part A, Pt nanoparticles supported on inactive SiO₂ are highly active for C=C bond hydrogenation, but are almost completely inactive for C=O bond hydrogenation. Comparing the rate of butyraldehyde formation with the combined rates of crotyl alcohol and butanol formation, Fig. 1A shows that Pt is more than 30 times more active for C=C bond hydrogenation compared to C=O bond hydrogenation. However, toward the goal of increasing the selectivity for C=O bond hydrogenation during selective partial hydrogenation, we have investigated the effect of coating the Pt nanoparticles with an overlayer of TiO₂. TiO₂ has previously been shown to be an active support for Pt leading to an increased rate of C=O bond hydrogenation.

Fig. 2 part B shows that when TiO₂ is deposited onto a film of Pt nanoparticles by atomic layer deposition, the rate of C=C bond hydrogenation decreases while the rate of C=O bond hydrogenation increases relative to the clean Pt nanoparticles. This shows the ability of the newly formed Pt–TiO₂ interface to increase the rate of C=O hydrogenation. Fig. 2B also shows that as the Pt surface is passivated with TiO₂, the rate of C=C bond hydrogenation decreases as expected. This is different than previous studies where metal nanoparticles are supported on TiO₂, which increases the rate

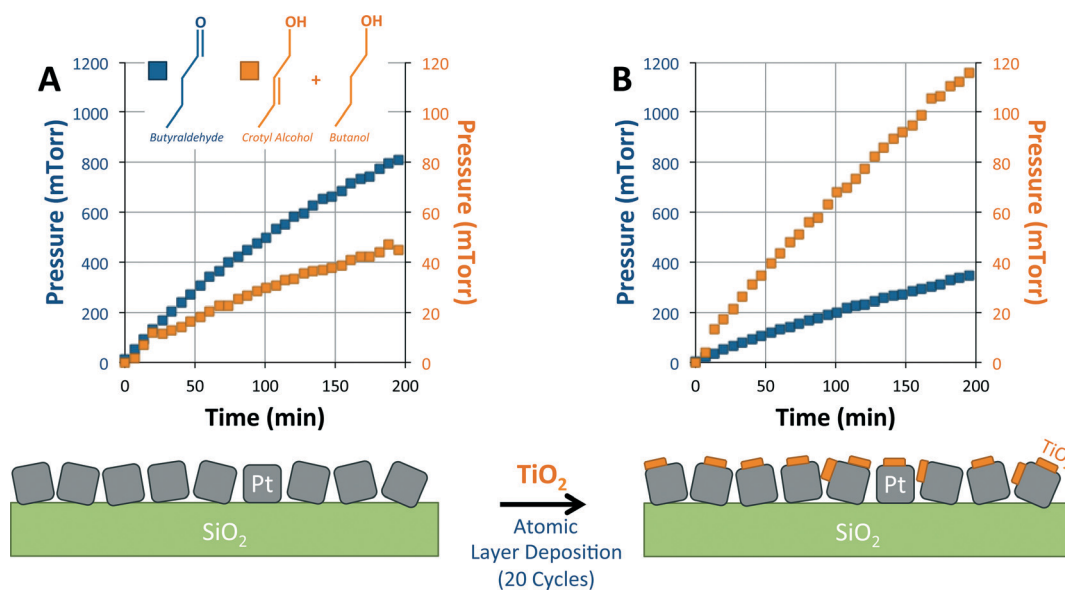


Fig. 2 Rate of formation of butyraldehyde (blue squares) and combined formation of crotyl alcohol and butanol (orange squares). Part A shows results for Pt nanoparticles deposited onto an SiO₂ substrate by LB deposition while part B shows results for identical Pt nanoparticles following 20 cycles of TiO₂ atomic layer deposition. As shown in part B, the TiO₂ overlayer decreases the C=C bond hydrogenation rate by more than a factor of 2 while increasing the C=O bond hydrogenation rate by a factor of almost 3.

of both C=C and C=O bond hydrogenation compared to an inactive SiO₂ support.

Fig. 3 shows the effect of increasing the TiO₂ overlayer thickness by additional ALD cycles on the kinetics of both C=C and C=O bond hydrogenation. For reference, Fig. 4 shows the atomic fraction of Pt:Ti measured by XPS for each overlayer coverage. Fig. 3 part A demonstrates that the rate of C=C bond hydrogenation decreases monotonically with increasing overlayer coverage as expected. However, part B shows that the rate of C=O bond hydrogenation initially increases by more than a factor of 5, reaching a maximum at 20 cycles, which corresponds to approximately a 1:1 ratio of Pt:Ti on the catalyst surface (see Fig. 4). Above this point, continuing to increase the coverage of TiO₂ leads to a decrease in the C=O bond hydrogenation rate. This loss in C=O bond hydrogenation activity is expected at oxide coverages above 50%, where both the total amount of exposed Pt sites as well as the number of Pt-TiO₂ interface sites will decrease with increasing oxide coverage.

This result is consistent with previous work by Boffa *et al.* on CO and CO₂ hydrogenation using a planar Rh catalyst decorated with a metal oxide. However, in those previous studies kinetics were only measured for single path reactions. If we assume that the rate of C=O bond hydrogenation scales with the number of oxide-metal interface sites while C=C bond hydrogenation scales with the total number of metal sites as suggested previously, then a trend toward higher selectivity for C=O bond hydrogenation would be expected with increasing oxide coverage, where at oxide coverages approaching unity, every exposed Pt site becomes an interface site. Consequently, using the rate of C=C bond hydrogenation as a measurement of the exposed Pt surface area, the important question here is how the rate of decrease

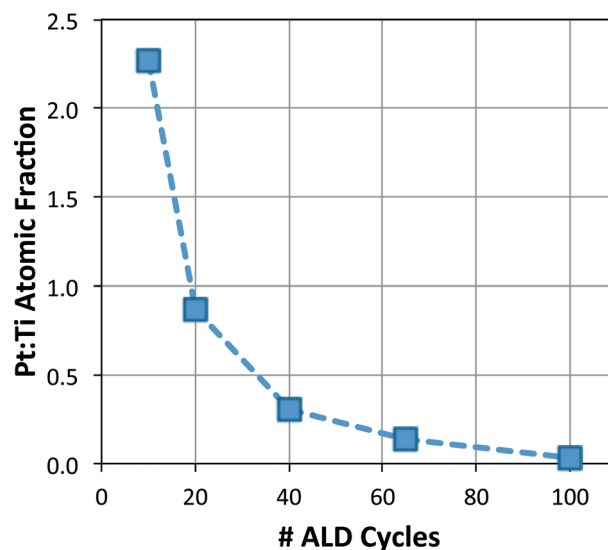


Fig. 4 Pt:Ti atomic fraction measured by XPS as a function of increasing cycles of TiO₂ atomic layer deposition.

in the C=O bond activity compares to the rate of decrease in the C=C bond activity, or in other words, how selectivity scales with increasing TiO₂ coverage.

Fig. 5 shows that the selectivity does not follow the predicted behavior based on a simple active sites argument. Rather we see that a maximum selectivity of approximately 20% is reached by 20 cycles, corresponding to the maximum rate of C=O bond hydrogenation. Above this coverage, it can be seen that the rate of C=O and C=C bond hydrogenation decreases in nearly exact proportion to one another. In these experiments the propylene selectivity was constant at approximately 30% (not shown). These results are not easily

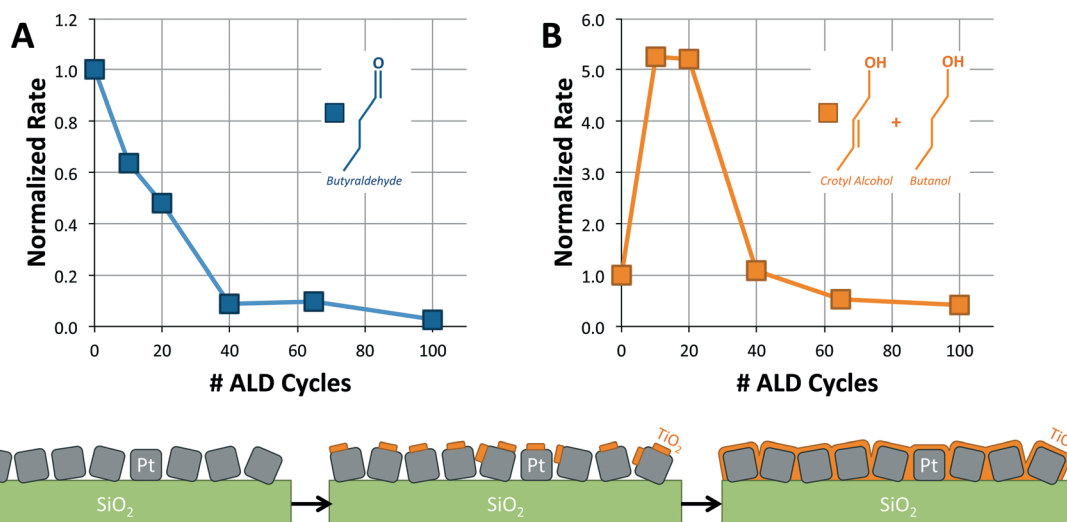


Fig. 3 Effect of increasing cycles of TiO₂ atomic layer deposition onto Pt nanoparticles. Part A shows the effect of increasing overlayer thickness on the rate of butyraldehyde formation while part B shows the effect on the combined rates of crotyl alcohol and butanol formation. As seen in part A, the C=C bond hydrogenation rate decreases monotonically as increasing ALD cycles progressively passivate the Pt surface with TiO₂. However, part B shows that the rate of C=O bond hydrogenation initially increases, reaching a maximum between 10 and 20 cycles before starting to decrease with decreasing Pt surface area.

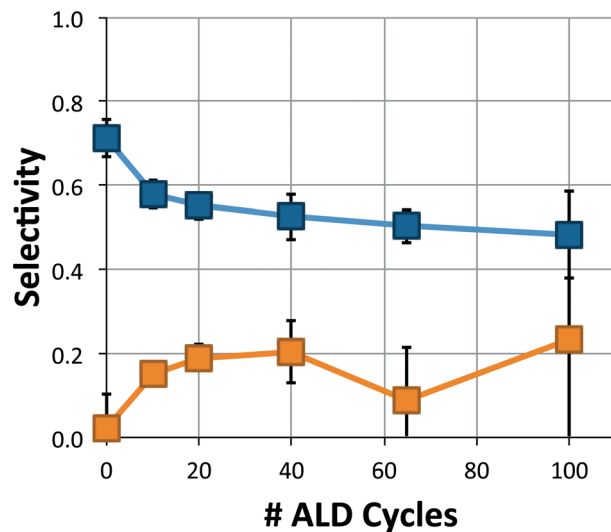


Fig. 5 Selectivity for butyraldehyde conversion (blue squares) and combined crotyl alcohol and butanol conversion (orange squares) for increasing TiO_2 coverage on Pt nanoparticles. Error bars represent 95% confidence intervals based on linear fits to the rate of product formation with time. Selectivity for $\text{C}=\text{O}$ bond hydrogenation initially increases reaching a maximum value of approximately 20% after 20 cycles of TiO_2 deposition. However, increasing oxide coverage beyond 20 cycles has little effect on the reaction selectivity. This trend in selectivity does not follow the expected ratio of interface sites to total Pt sites, indicating that the rate limiting step in selective $\text{C}=\text{O}$ bond hydrogenation does not occur at the $\text{Pt}-\text{TiO}_2$ interface. In these experiments the propylene selectivity stayed constant at approximately 30% (not shown).

explained by considering a single rate limiting reaction step for $\text{C}=\text{O}$ bond occurring at the $\text{Pt}-\text{TiO}_2$ interface for all oxide coverages. Rather these results are consistent with a reaction mechanism for $\text{C}=\text{O}$ bond hydrogenation that is initially rate limited by the density of oxide–metal interface sites while oxide coverage is low, but becomes rate limited by accessible Pt at high oxide coverage. As discussed above, this could be the result of limited H_2 dissociation activity on catalysts where very little Pt is exposed. Alternatively, this could be explained by a reverse spillover reaction mechanism where crotyl-oxy intermediates that form on TiO_2 migrate to Pt where they subsequently react to produce crotyl alcohol.

Although elemental composition of these samples is measured by XPS (see Fig. 4), imaging the morphology of these oxide films by electron microscopy is difficult owing to the low contrast of TiO_2 on Pt. Accordingly, we cannot be certain that these kinetics are not partially the result of a complex morphology of the TiO_2 film as it deposits on the Pt nanoparticle catalysts during ALD. Consequently, to confirm the above conclusions, it is desirable to study a catalyst where it is possible to independently control the density of interface sites and the total number of metal sites.

3.2. Discrete CeO_2 nanocubes on Pt thin films

To accomplish this, we have also investigated deposition of colloidal CeO_2 nanoparticles onto a Pt thin film catalyst.

CeO_2 has been shown to also act as an active support for Pt, increasing the activity of $\text{C}=\text{O}$ bond hydrogenation on supported metal catalysts similar to $\text{Pt}-\text{TiO}_2$.^{30–32} In this experiment, we select CeO_2 rather than TiO_2 because it is possible to synthesize monodisperse CeO_2 nanoparticles with a cubic geometry (see Fig. 1B) such that each nanocube will experience good contact with the Pt surface.¹⁴ In this system the number of $\text{Pt}-\text{CeO}_2$ interface sites scales linearly with the coverage of CeO_2 nanocubes on the Pt thin film, while the number of Pt sites scales as 1 minus the coverage of CeO_2 nanocubes.

Consequently, by measuring the kinetics of $\text{C}=\text{O}$ bond hydrogenation in this system as a function of oxide coverage, it is possible to confirm that Pt surface area rather than oxide–metal interface sites becomes rate limiting for $\text{C}=\text{O}$ bond hydrogenation at high oxide coverage. Specifically, if the rate of $\text{C}=\text{O}$ bond hydrogenation scales linearly with increasing nanoparticle coverage, this would suggest that the rate limiting step for $\text{C}=\text{O}$ bond activation occurs at the oxide–metal interface independent of oxide coverage. On the other hand, if the rate of $\text{C}=\text{O}$ bond hydrogenation is shown to decrease at high coverage even though the CeO_2 nanocubes remain discrete, this would confirm that the rate of $\text{C}=\text{O}$ bond hydrogenation becomes limited by the accessible Pt surface area rather than the density of oxide–metal interface sites at high oxide coverage.

To systematically control the coverage of CeO_2 nanocubes on the surface of the Pt catalyst, we used LB deposition. The CeO_2 nanoparticle coverage of the resulting films was characterized by both XPS and TEM. Fig. 6 shows the Pt:Ce atomic fraction of the catalyst surface measured by XPS as a function of film compression during LB deposition. Care was taken to ensure that the nanoparticles deposited homogeneously rather than as rafts of self-assembled clusters, which sometimes occurred if the nanoparticles were washed too many times following synthesis. Fig. 7 shows TEM images of CeO_2 nanoparticle films deposited by LB at four different compressions confirming that the nanoparticle dispersion in these samples is quite homogeneous, even on the nanoscale. All catalysts were cleaned following deposition by UV ozone to remove the oleic acid capping agent from the CeO_2 nanoparticles by a previously established method.²² Additional TEM was performed to confirm that this cleaning method as well as subsequent reaction conditions does not lead to melting or agglomeration of the CeO_2 nanoparticles.

Fig. 8 shows the results of kinetic studies of these catalysts for crotonaldehyde hydrogenation. Part A shows the normalized rate of crotyl alcohol formation as a function of CeO_2 nanoparticle coverage, while part B shows the corresponding reaction selectivity to each of the four measured products. Results from Fig. 8A demonstrate that there is an approximately 10-fold increase in the rate of $\text{C}=\text{O}$ bond hydrogenation on the $\text{Pt}-\text{CeO}_2$ catalyst initially compared to the Pt catalyst without CeO_2 . However, as in the case with the TiO_2 coverage experiment described above, the rate of $\text{C}=\text{O}$ bond hydrogenation subsequently decreases with increasing CeO_2

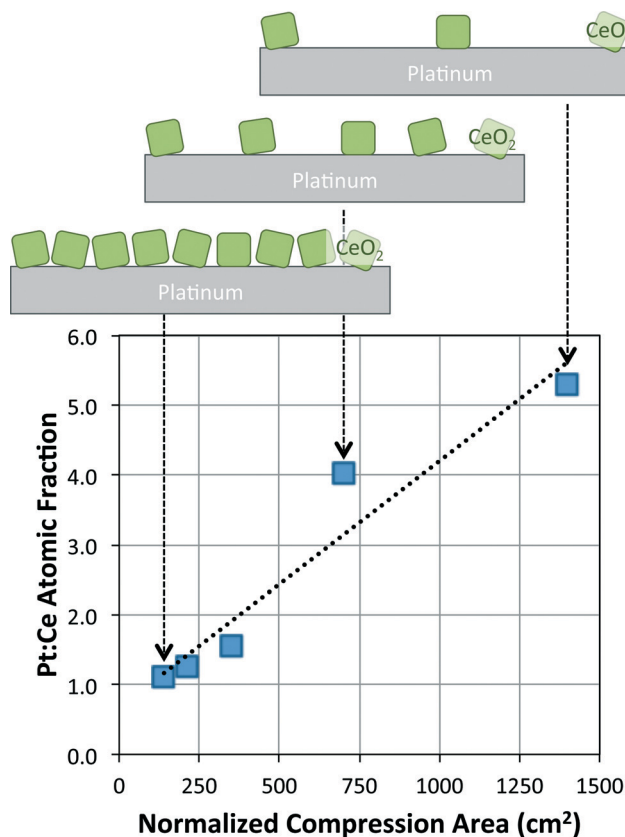


Fig. 6 Pt:Ce atomic fraction measured by XPS as a function of CeO₂ nanoparticle compression during LB deposition onto a Pt thin film catalyst. The surface area of the LB trough can be controlled between 65 and 485 cm². To measure the atomic fraction of particles at compression areas greater than 485 cm², a proportionally lesser volume of the CeO₂ nanoparticle suspension was dispersed onto the trough to give an effective increase in the surface area per particle.

nanoparticle coverage, eventually dropping to less than half of its maximum activity at the highest coverage tested. This observation is inconsistent with the hypothesis that selective C=O bond hydrogenation is rate limited by the Pt–CeO₂ interface independent of oxide coverage. Rather this data supports the conclusion that Pt surface area becomes rate limiting for selective C=O bond hydrogenation when the oxide coverage is high. Fig. 8 part B shows the effect of CeO₂ nanoparticle coverage on the catalyst selectivity. Consistent with the observations described above, the selectivity for C=O hydrogenation does not increase monotonically with nanoparticle coverage as would be expected for a rate limiting step occurring at the Pt–CeO₂ interface independent of oxide coverage.

We also observed that unlike the case of TiO₂ on Pt, the rate of C=C bond hydrogenation did not decrease significantly with increasing CeO₂ nanoparticle coverage, and in some cases C=C bond hydrogenation rates even increased at high CeO₂ coverages relative to a clean Pt surface. This observation led us to investigate the possibility that CeO₂ promotes the isomerization of crotyl alcohol to butyraldehyde. However, the results of these experiments (not shown) indicate

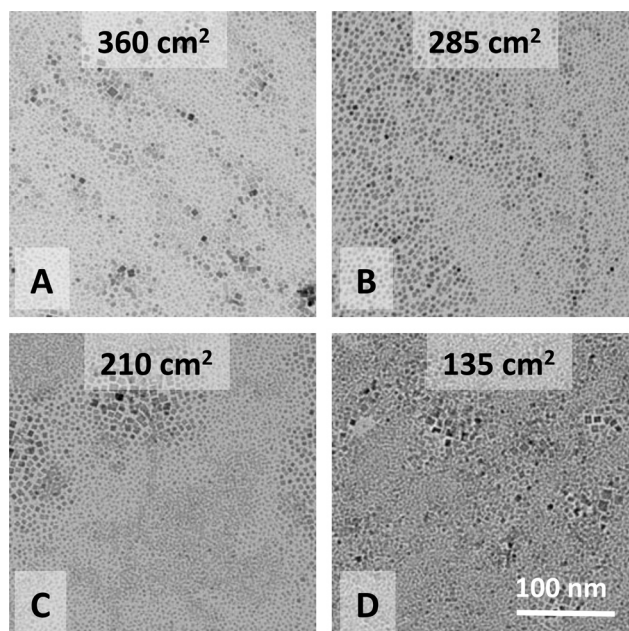


Fig. 7 TEM images of CeO₂ nanoparticle films deposited by LB at film compressions corresponding to 360 cm² (A), 285 cm² (B), 210 cm² (C), and 135 cm² (D).

that CeO₂ plays no role in enhancing this isomerization pathway. Instead, we found that when the rate of ethylene hydrogenation was measured immediately following crotonaldehyde hydrogenation, without exposing the catalyst to ambient atmosphere, the rate was significantly lower than for a fresh catalyst. We also observed that post-reaction the rate of ethylene hydrogenation was higher on a Pt–CeO₂ catalyst compared to a clean Pt thin film. We attribute this to CO deposition on the Pt catalyst during crotonaldehyde hydrogenation, where CO is a byproduct of the decarbonylation pathway shown in Scheme 1. CO poisoning of the Pt surface significantly decreases the rate of C=C bond hydrogenation, and we find that exposing the catalyst to air at room temperature following crotonaldehyde hydrogenation is sufficient to remove the deposited CO and restore the original catalyst activity for ethylene hydrogenation. Consequently, if we recognize that the Pt surface is partially CO poisoned during reaction by the decarbonylation of crotonaldehyde to propylene, then it is not surprising that the CeO₂ covered surface would be more active for butyraldehyde hydrogenation compared to the clean Pt film. This is because the oxide–metal interface is relatively resistant to CO poisoning compared to a clean Pt surface.³³

3.3. Pt-on-CeO₂ and CeO₂-on-Pt nanocube bilayers

To further confirm that Pt sites rather than interfacial sites become rate limiting for selective C=O bond hydrogenation at high oxide coverage, we lastly investigated tandem bilayers of Pt and CeO₂ cubic nanoparticles. For these studies four catalysts were prepared on an SiO₂ substrate: A) CeO₂ nanoparticles alone, B) Pt nanoparticles alone, C) CeO₂

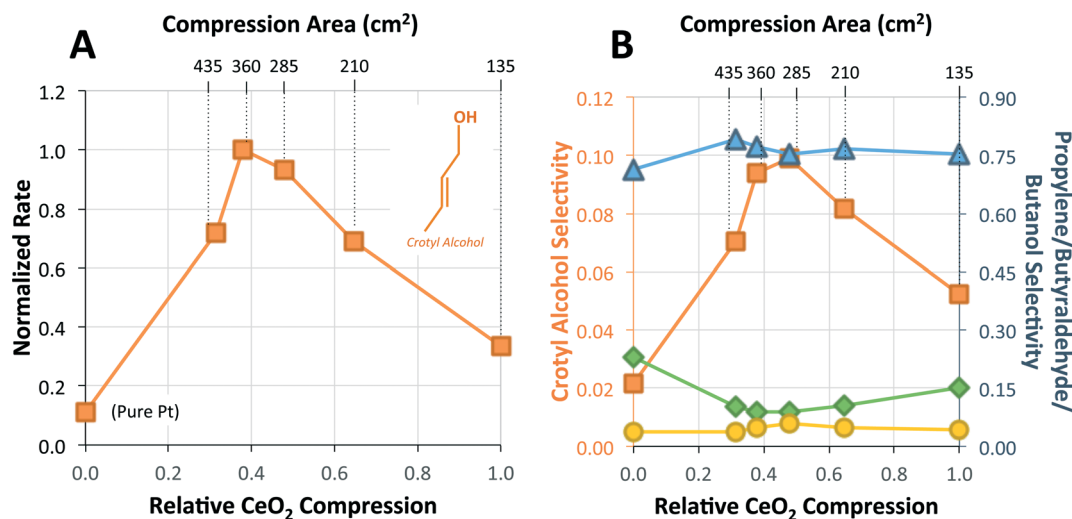


Fig. 8 Kinetics of crotonaldehyde hydrogenation on CeO₂ nanoparticles deposited onto a Pt thin film catalyst as a function of CeO₂ coverage. Part A shows the normalized rate of crotyl alcohol formation as a function of film coverage. Part B shows the corresponding selectivity for each of the four reaction products: orange squares show crotyl alcohol, blue triangles show butyraldehyde, green diamonds show propylene, and yellow circles show butanol.

nanoparticles deposited on top of a Pt nanoparticle film, and D) Pt nanoparticles deposited on top of a CeO₂ nanoparticle film. These catalysts were prepared by single (A and B) or tandem (C and D) LB depositions. As in all LB experiments, substrates were cleaned by UV ozone prior to LB deposition to make the surface hydrophilic. In the case of the tandem depositions, UV cleaning was also performed as an intermediate step between depositions to remove the capping agent from the bottom layer and to make the surface hydrophilic in order to ensure good coverage of the top nanoparticle film. Because CeO₂ and Pt nanoparticle films are each deposited at the maximum surface pressure (*i.e.* highest coverage) prior to multilayer formation, the coverage and packing of both types of particles was similar between the four samples.

The results of these experiments are shown in Fig. 9, and these results are schematically summarized in Fig. 10. These

data indicate that, as expected, CeO₂ is inactive in the absence of Pt, while Pt alone is active primarily for C=C bond hydrogenation. However, we find that only the Pt-on-CeO₂ catalyst is active for C=O bond hydrogenation, while the CeO₂-on-Pt catalyst shows no enhancement of the C=O bond hydrogenation pathway compared to Pt alone. This result is entirely consistent with the previous observations that at high oxide coverage on Pt, C=O bond hydrogenation appears to be rate limited by the area of accessible Pt near an active oxide-metal interface as opposed to the actual number of interface sites present in the catalyst.

3.4. Role of Pt beyond the oxide-metal interface

Numerous previous studies have accurately demonstrated the critical role of the oxide-metal interface in selective C=O

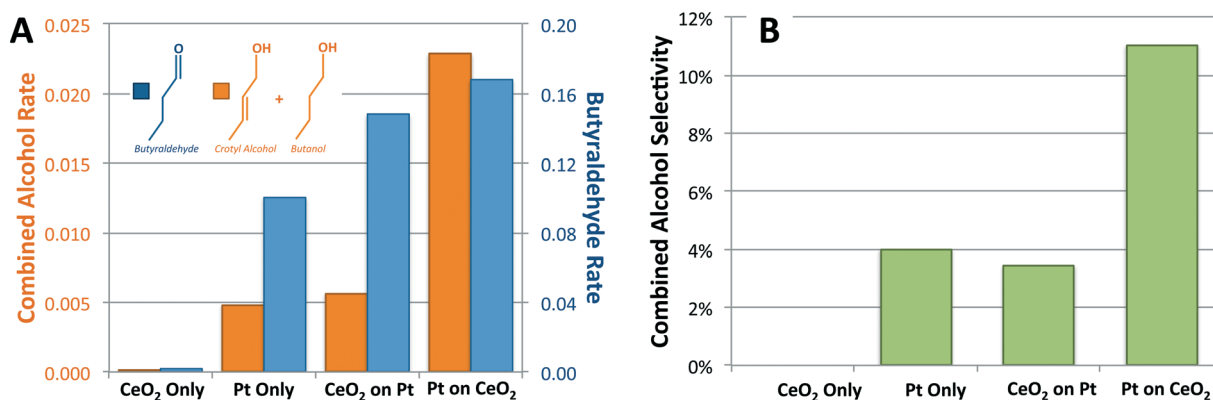


Fig. 9 Kinetics of crotonaldehyde hydrogenation on 1) CeO₂ nanoparticles, 2) Pt nanoparticles, 3) CeO₂-on-Pt nanoparticle bilayer, and 4) Pt-on-CeO₂ nanoparticle bilayer. Part A shows the combined rate of crotyl alcohol and butanol formation (orange bars) and the rate of butyraldehyde formation (blue bars). Rates are given in turnover frequency units (molecules produced per site per second) assuming 10¹⁵ active sites per cm². Although this is approximate, it provides a consistent normalization factor for comparing these four catalyst systems. Part B shows the combined selectivity to crotyl alcohol and butanol for each of these four catalysts.

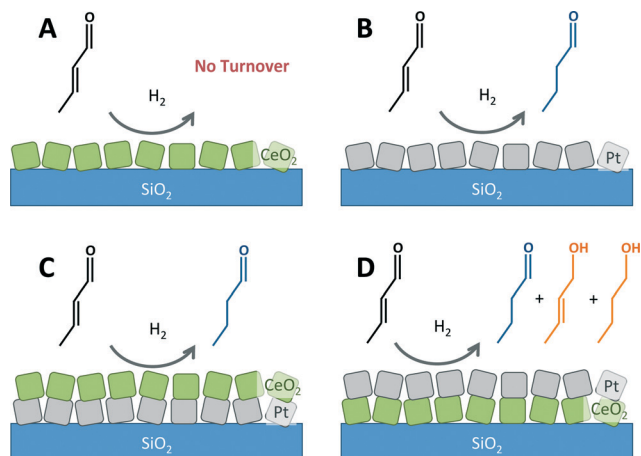


Fig. 10 Schematic summary of experimental results given in Fig. 9. CeO₂ alone is not active for any reaction product (A); Pt alone is active predominantly for C=C bond hydrogenation (B); CeO₂-on-Pt is also active predominantly for C=C bond hydrogenation (C). However, only Pt-on-CeO₂ shows an enhanced rate for C=O bond hydrogenation compared to the other 3 catalysts (D). This result suggests the need for a high surface area of exposed Pt within some distance of the Pt–CeO₂ interface to catalyze the C=O hydrogenation pathway.

bond activation. The results of the present study now illustrate an additional consideration in catalyst design that also affects the kinetics of C=O bond hydrogenation at or near the active oxide–metal interface, namely the accessible Pt surface area extending beyond the oxide phase. Although, the exact mechanism of this observation remains under investigation, we consider two plausible explanations here.

First, it is well known that in supported Pt catalysts, one role of Pt is to dissociate H₂ to form atomic H that may subsequently spillover to the oxide support.^{26,27,34} Consequently, we have considered the possibility that the observed kinetics for selective C=O bond hydrogenation represent the need for bulk Pt sites to produce a sufficient supply of atomic H to the oxide–metal interface where selective C=O bond hydrogenation may subsequently occur. We further note that reduction of the oxide surface by H spillover is believed to be critical for activating the oxide catalysts for selective C=O bond hydrogenation. Specifically, recent experimental and theoretical studies show that O vacancy sites on the oxide surface are responsible for the electronic activation of the C=O bond *via* a charge transfer interaction with the adsorbed aldehyde.²² Consequently, it is likely that a limited supply of atomic H on catalysts with high oxide coverage also influences the electronic structure of the oxide itself. Specifically, TiO₂ and CeO₂ may not be activated during reaction conditions on catalysts where insufficient Pt surface is present to reduce the metal oxide surface and generate a high concentration of O vacancy states *via* H spillover.

To test this hypothesis we have analyzed XPS spectra of post-reaction catalysts and observe that consistent with this proposed explanation, the fraction of reduced Ce³⁺ sites on the catalyst following reaction varies with the absolute CeO₂ nanoparticle coverage. Fig. 11 shows the fraction of reduced

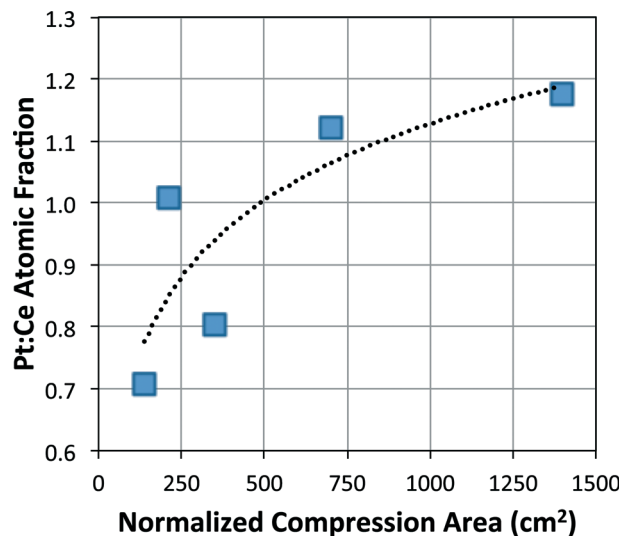


Fig. 11 Ce³⁺:Ce⁴⁺ atomic fraction measured by XPS as a function of CeO₂ nanoparticle compression during LB deposition onto a Pt thin film catalyst.

Ce³⁺ to fully oxidized Ce⁴⁺ sites as a function of CeO₂ nanoparticle coverage on a Pt film following reaction. It can be seen that the density of O vacancies corresponding to Ce³⁺ sites is greatest for catalysts with low CeO₂ nanoparticle coverage and that the density of O vacancy sites decreases for catalysts with high CeO₂ coverage. This data is consistent with the hypothesis that an insufficient supply of atomic H from Pt to the CeO₂ nanoparticles in samples with high oxide coverage may limit the activity of C=O bond hydrogenation in these catalysts by failing to fully activate the oxide phase.

Alternately, we consider the possibility that the formation of crotyl alcohol may actually occur on Pt following the reverse spillover of a crotyl-oxy intermediate. It has previously been shown that C=O bond activation occurs by a charge transfer interaction at O-vacancy sites on a reducible oxide.²² Addition of one H atom to the carbonyl C of this activated species produces an alkoxy intermediate that is bound to the oxide surface *via* the terminal O, and this species has been detected on a TiO₂ surface by SFG vibrational spectroscopy during both crotonaldehyde²⁰ and furfuraldehyde²² hydrogenation. Additionally, atomic resolution STM studies have reported the observed spillover of alkoxy intermediates across the Pt–TiO₂ interface.³⁵ Consequently, it is plausible that selective C=O bond hydrogenation may occur by the reverse spillover of an activated alkoxy intermediate from the oxide surface onto the Pt. If this is true, then the present results would suggest that subsequent hydrogenation of the alkoxy intermediate to the alcohol product is actually rate limiting in this reaction and occurs on the Pt surface within some length scale determined by its mean diffusional free path under reaction conditions. Although this mechanism admittedly breaks with the predominant belief that the oxide–metal interface is the active site for selective C=O bond hydrogenation, this mechanism could explain the dependence of catalytic selectivity on oxide electronic structure^{23,25} since

the metal oxide is responsible for formation of the active crotyl-oxy intermediate as well as the need for an active oxide-metal interface^{22,24} since this interface is required for the reverse spillover of crotyl-oxy from TiO₂ (or CeO₂) to Pt. Further studies are needed to differentiate between these two explanations for the consistent observation that at high oxide coverage, Pt surface area becomes rate limiting for C=O bond hydrogenation.

4. Conclusions

We have measured the kinetics of crotonaldehyde hydrogenation by multiple oxide-on-metal catalyst systems consisting of both Pt-TiO₂ and Pt-CeO₂. In each case we find that the rate of selective C=O bond hydrogenation is enhanced by the presence of an oxide-metal interface, but that the kinetics of this selective reaction pathway become limited by the area of accessible Pt at high oxide coverage. These results indicate a fundamental limitation in the partial hydrogenation selectivity of unsaturated aldehydes that can be achieved using a Pt catalyst. Passivating a Pt catalyst using an active TiO₂ overlayer can decrease the rate of competing C=C bond hydrogenation but this eventually leads to an equal decrease in the rate of C=O bond hydrogenation. The net result is that reaction selectivity only depends on the oxide layer at low coverage, while at high coverage the selectivity for C=O bond hydrogenation reaches a maximum that is independent of the TiO₂ coverage. A similar result was demonstrated for CeO₂ on Pt, where the rate of C=O bond hydrogenation initially increases with CeO₂ coverage relative to a clean Pt film and then decreases again at high CeO₂ coverage. In bilayer catalysts consisting of CeO₂ and Pt nanocubes, we find that both Pt-on-CeO₂ and CeO₂-on-Pt are active for C=C bond hydrogenation, while only Pt-on-CeO₂ is active for C=O bond hydrogenation. These results consistently show that the Pt surface area beyond the oxide-metal interface can limit the rate of C=O bond hydrogenation on catalysts where the Pt surface area is low and the oxide coverage is high. These findings improve mechanistic understanding of catalytic selectivity on bifunctional nanoparticle surfaces and provide an important design parameter for tuning catalyst performance for partial hydrogenation selectivity.

Acknowledgements

X. Y. and Q. A. B. were supported by the Air Force Office of Scientific Research under award FA9550-15-1-0204 granted to L. R. B. This work was also supported by the OSU Department of Chemistry and Biochemistry through junior faculty funds for L. R. B. Electron beam evaporation and atomic layer deposition were performed at the OSU Nanotech West Laboratory. XPS was performed at the OSU Surface Analysis Laboratory. Langmuir-Blodgett deposition was performed at the OSU Nanosystems Laboratory. Electron microscopy was performed at the OSU Center for Electron Microscopy and Analysis

(CEMAS). The authors gratefully acknowledge Hendrik Colijn for assistance with electron microscopy.

References

- 1 R. A. Sheldon, E factors, green chemistry and catalysis: an odyssey, *Chem. Commun.*, 2008, 3352–3365.
- 2 R. A. Sheldon, Fundamentals of green chemistry: efficiency in reaction design, *Chem. Soc. Rev.*, 2012, **41**, 1437–1451.
- 3 A. Elgowainy, *et al.*, Energy Efficiency and Greenhouse Gas Emission Intensity of Petroleum Products at U.S. Refineries, *Environ. Sci. Technol.*, 2014, **48**, 7612–7624.
- 4 D. R. Strongin, J. Carrazza, S. R. Bare and G. A. Somorjai, The importance of C7 sites and surface roughness in the ammonia synthesis reaction over iron, *J. Catal.*, 1987, **103**, 213–215.
- 5 S. Alayoglu, C. Aliaga, C. Sprung and G. Somorjai, Size and Shape Dependence on Pt Nanoparticles for the Methylcyclopentane/Hydrogen Ring Opening/Ring Enlargement Reaction, *Catal. Lett.*, 2011, **141**, 914–924.
- 6 M. S. Chen and D. W. Goodman, The structure of catalytically active gold on titania, *Science*, 2004, **306**, 252–255.
- 7 R. M. Rioux, H. Song, J. D. Hoefelmeyer, P. Yang and G. A. Somorjai, High-surface-area catalyst design: Synthesis, characterization, and reaction studies of platinum nanoparticles in mesoporous SBA-15 silica, *J. Phys. Chem. B*, 2005, **109**, 2192–2202.
- 8 M. Valden, X. Lai and D. W. Goodman, Onset of Catalytic Activity of Gold Clusters on Titania with the Appearance of Nonmetallic Properties, *Science*, 1998, **281**, 1647–1650.
- 9 V. A. Bondzie, S. C. Parker and C. T. Campbell, The kinetics of CO oxidation by adsorbed oxygen on well-defined gold particles on TiO₂(110), *Catal. Lett.*, 1999, **63**, 143–151.
- 10 D. Goodman, “Catalytically active Au on Titania:” yet another example of a strong metal support interaction (SMSI)?, *Catal. Lett.*, 2005, **99**, 1–4.
- 11 R. M. Lambert, R. L. Cropley, A. Husain and M. S. Tikhov, Halogen-induced selectivity in heterogeneous epoxidation is an electronic effect - fluorine, chlorine, bromine and iodine in the Ag-catalysed selective oxidation of ethene, *Chem. Commun.*, 2003, 1184–1185.
- 12 P. Landon, P. J. Collier, A. J. Papworth, C. J. Kiely and G. J. Hutchings, Direct formation of hydrogen peroxide from H₂/O₂ using a gold catalyst, *Chem. Commun.*, 2002, 2058–2059.
- 13 J. K. Edwards, *et al.*, Direct synthesis of hydrogen peroxide from H₂ and O₂ using TiO₂-supported Au-Pd catalysts, *J. Catal.*, 2005, **236**, 69–79.
- 14 Y. Yamada, *et al.*, Nanocrystal bilayer for tandem catalysis, *Nat. Chem.*, 2011, **3**, 372–376.
- 15 M. A. Vannice and B. Sen, Metal-support effects on the intramolecular selectivity of crotonaldehyde hydrogenation over platinum, *J. Catal.*, 1989, **115**, 65–78.
- 16 D. G. Blackmond, R. Oukaci, B. Blanc and P. Gallezot, Geometric and electronic effects in the selective hydrogenation of α,β -unsaturated aldehydes over zeolite-supported metals, *J. Catal.*, 1991, **131**, 401–411.

- 17 S. D. Lin, D. K. Sanders and M. A. Vannice, Influence of metal-support effects on acetophenone hydrogenation over platinum, *Appl. Catal., A*, 1994, **113**, 59–73.
- 18 J. Kijeński and P. Winiarek, Selective hydrogenation of α,β -unsaturated aldehydes over Pt catalysts deposited on monolayer supports, *Appl. Catal., A*, 2000, **193**, L1–L4.
- 19 R. Malathi and R. P. Viswanath, Citral hydrogenation on supported platinum catalysts, *Appl. Catal., A*, 2001, **208**, 323–327.
- 20 G. Kennedy, L. R. Baker and G. A. Somorjai, Selective Amplification of C=O Bond Hydrogenation on Pt/TiO₂: Catalytic Reaction and Sum-Frequency Generation Vibrational Spectroscopy Studies of Crotonaldehyde Hydrogenation, *Angew. Chem., Int. Ed.*, 2014, **53**, 3405–3408.
- 21 C. J. Kliewer, M. Bieri and G. A. Somorjai, Hydrogenation of the α,β -Unsaturated Aldehydes Acrolein, Crotonaldehyde, and Prenal over Pt Single Crystals: A Kinetic and Sum-Frequency Generation Vibrational Spectroscopy Study, *J. Am. Chem. Soc.*, 2009, **131**, 9958–9966.
- 22 L. R. Baker, *et al.*, Furfuraldehyde Hydrogenation on Titanium Oxide-Supported Platinum Nanoparticles Studied by Sum Frequency Generation Vibrational Spectroscopy: Acid-Base Catalysis Explains the Molecular Origin of Strong Metal-Support Interactions, *J. Am. Chem. Soc.*, 2012, **134**, 14208–14216.
- 23 A. Boffa, C. Lin, A. T. Bell and G. A. Somorjai, Promotion of CO and CO₂ Hydrogenation over Rh by Metal Oxides: The Influence of Oxide Lewis Acidity and Reducibility, *J. Catal.*, 1994, **149**, 149–158.
- 24 A. B. Boffa, A. T. Bell and G. A. Somorjai, Vanadium Oxide Deposited on an Rh Foil: CO and CO₂ Hydrogenation Reactivity, *J. Catal.*, 1993, **139**, 602–610.
- 25 A. B. Boffa, C. Lin, A. T. Bell and G. A. Somorjai, Lewis acidity as an explanation for oxide promotion of metals: implications of its importance and limits for catalytic reactions, *Catal. Lett.*, 1994, **27**, 243–249.
- 26 W. C. Conner and J. L. Falconer, Spillover in Heterogeneous Catalysis, *Chem. Rev.*, 1995, **95**, 759–788.
- 27 A. J. Du, S. C. Smith, X. D. Yao and G. Q. Lu, Hydrogen Spillover Mechanism on a Pd-Doped Mg Surface as Revealed by ab initio Density Functional Calculation, *J. Am. Chem. Soc.*, 2007, **129**, 10201–10204.
- 28 C.-K. Tsung, *et al.*, Sub-10 nm Platinum Nanocrystals with Size and Shape Control: Catalytic Study for Ethylene and Pyrrole Hydrogenation, *J. Am. Chem. Soc.*, 2009, **131**, 5816–5822.
- 29 S. Yang and L. Gao, Controlled Synthesis and Self-Assembly of CeO₂ Nanocubes, *J. Am. Chem. Soc.*, 2006, **128**, 9330–9331.
- 30 M. Abid, V. Paul-Boncour and R. Touroude, Pt/CeO₂ catalysts in crotonaldehyde hydrogenation: Selectivity, metal particle size and SMSI states, *Appl. Catal., A*, 2006, **297**, 48–59.
- 31 C. Mazzocchia, *et al.*, Hydrogenation of CO over Rh/SiO₂-CeO₂ catalysts: kinetic evidences, *J. Mol. Catal. A: Chem.*, 2001, **165**, 219–230.
- 32 A. Trovarelli, C. de Leitenburg and G. Dolcetti, CO and CO₂ hydrogenation under transient conditions over Rh-CeO₂: novel positive effects of metal-support interaction on catalytic activity and selectivity, *J. Chem. Soc., Chem. Commun.*, 1991, 472–473.
- 33 A. M. Contreras, J. Grunes, X.-M. Yan, A. Liddle and G. A. Somorjai, Fabrication of 2-dimensional platinum nanocatalyst arrays by electron beam lithography: ethylene hydrogenation and CO-poisoning reaction studies, *Top. Catal.*, 2006, **39**, 123–129.
- 34 R. Prins, Hydrogen Spillover Facts and Fiction, *Chem. Rev.*, 2012, **112**, 2714–2738.
- 35 S. Takakusagi, K.-I. Fukui, R. Tero, K. Asakura and Y. Iwasawa, First Direct Visualization of Spillover Species Emitted from Pt Nanoparticles†, *Langmuir*, 2010, **26**, 16392–16396.